Tc(III) character, and thus its signal appears farther away from the Tc(I) region and further into the Tc(III) region.

Acknowledgment. We thank Dr. Nadine deVries for preparing the CNMe, Dr. William Davis for his advice on the X-ray crystallography, and Dr. Catherine Costello and Chen-hui Zeng of the NIH Northeast Regional Mass Spectrometry Facility for their work on the mass spectra. Partial financial support was provided by USPHS Grant No. 5 R01 CA34970 and DOE Grant No. DE-FG02-87ER60526.

Supplementary Material Available: Tables SI-SV, listing respectively complete X-ray data, hydrogen atom positional parameters, intramolecular atomic distances involving the non-hydrogen atoms, intramolecular bond angles, and anisotropic thermal parameters (8 pages); Table SVI, listing calculated and observed structure factors (7 pages). Ordering information is given on any current masthead page.

Contribution from the Department of Chemistry, D-006, University of California at San Diego, La Jolla, California 92093-0506, Microcalorimetry Research Center, Faculty of Science, Osaka University, Toyonaka, Osaka 560, Japan, Department of Chemistry, University of Louisville, Louisville, Kentucky 40292, Department of Chemistry, University of Delaware, Newark, Delaware 19716, and School of Chemical Sciences, University of Illinois, Urbana, Illinois 61801

Effect of Quenched Disorder on Phase Transitions in the Mixed-Valence Solid Solution $[Fe^{III}_2Fe^{II}_{1-x}Co^{II}_xO(O_2CCH_3)_6(py)_3](py)$†

Ho G. Jang,[1] Kazutoshi Kaji,[2] Michio Sorai,*[,2] Richard J. Wittebort,*[,3] Steven J. Geib,[4] Arnold L. Rheingold,[4] and David N. Hendrickson*[,5]

Received January 24, 1990

The effect of adding permanently distorted $[Fe^{III}_2Co^{II}O(O_2CCH_3)_6(py)_3](py)$ (**2**) complexes to the lattice of the isostructural mixed-valence $Fe^{III}_2Fe^{II}O$ complex **1** to form solid solutions of $[Fe^{III}_2Fe^{II}_{1-x}Co^{II}_xO(O_2CCH_3)_6(py)_3](py)$ is examined. Single-crystal 298 K X-ray structures are presented for $[Fe_3O(O_2CCH_3)_6(py)_3](py)$ (**1**) and $Fe^{III}_2Co^{II}O$ complex **2**. Both complexes crystallize in the rhombohedral space group $R32$. Complex **1** has a unit cell with a = 17.558 (7) Å and c = 11.074 (4) Å, where Z = 3. Complex **2** crystallizes with a unit cell of a = 17.583 (6) Å and c = 11.074 (3) Å, with Z = 3. Complex **2** is statically disordered, whereas complex **1** is dynamically disordered at 298 K. In both cases Fe_2MO (M = Fe, Co) complexes and pyridine solvate molecules are alternatively stacked along the crystallographic C_3 axis. Each Fe_2MO and pyridine solvate molecule is at a 32 symmetry site, when the effects of the disorder are considered. Powder XRD data for **1**, **2**, and the x = 0.5 solid solution (complex **3**) show that complex **3** is indeed a solid solution and not just a mixture of crystals of **1** and **2**. Adiabatic calorimetry was used to measure the heat capacity at constant pressure, C_P, in the 12-300 K range for a 17.4981-g sample of complex **2** and a 13.6562-g sample of complex **3**. For the x = 0.5 solid solution complex **3** three C_P peaks were seen at 84.5, 148.0, and 168.8 K. A single broad C_P peak was seen at 148.5 K for $Fe^{III}_2Co^{II}$ complex **2**. This one broad peak gave a total entropy gain for the phase transition of 10.32 J K^{-1} mol^{-1}, which is close to a value of $\Delta S = R \ln 3$ = 9.13 J K^{-1} mol^{-1}. Solid-state ^2H NMR results for randomly oriented polycrystalline and magnetically oriented microcrystalline samples of **2** confirmed that the 148.5 K phase transition for $Fe^{III}_2Co^{II}$ complex **2** is due only to a cooperative onset of motion of the pyridine solvate molecules. The total entropy gain for the x = 0.5 solid solution was calculated to be ΔS = 19.74 J K^{-1} mol^{-1}. This ΔS value is rationalized in terms of the onset of valence detrapping in the Fe_2O complexes and pyridine solvate molecules in the solid-solution complex **3**. In agreement with the heat capacity results, ^{57}Fe Mössbauer data for $[Fe^{III}_2Fe^{II}_{1-x}Co^{II}_xO(O_2CCH_3)_6(py)_3](py)$ show that this solid solution converts from a ferrodistortive phase to a antiferrodistortive phase at ~85 K, finally to be completely valence detrapped and dynamic in a paradistortive phase at ~175 K. The $Fe^{III}_2Co^{II}O$ complexes in the solid-solution complex **3** behave as an unusual type of quenched disorder. They do not serve simply as lattice sites missing a mixed-valence Fe_3O complex. Each $Fe^{III}_2Co^{II}O$ complex is permanently distorted, and due to py···py contacts with neighboring trinuclear complexes it acts as an unusual element of disorder that appears to prohibit the appearance of an ordered state at a concentration of $Fe^{III}_2Co^{II}O$ complex below that predicted by percolation theory.

Introduction

In the solid state several mixed-valence complexes have been shown to convert from being valence trapped at low temperatures to valence detrapped at high temperatures. A valence-detrapped complex is rapidly interconverting between the different minima on its ground-state potential-energy surface. Mixed-valence biferrocenes[6] and trinuclear iron acetates[7] of the composition $[Fe^{III}_2Fe^{II}O(O_2CCH_3)_6(L)_3]S$, where L is a ligand and S is a solvate molecule, are some of the best studied complexes that valence detrap in the solid state. Valence detrapping of biferrocenium triiodide has been shown[8] to occur cooperatively in a phase transition by means of heat capacity measurements. The presence of valence-detrapping phase transitions has also been established with this same technique for several $[Fe^{III}_2Fe^{II}O(O_2CCH_3)_6(L)_3]S$ complexes.[7a,b,g,h] Intermolecular interactions are present between pairs of Fe_3O complexes due to the overlap of two L = pyridine ligands. As a result, long-range order develops and valence detrapping occurs cooperatively in large regions (domains) of each crystal.

† Calorimetric part of this paper corresponds to Contribution No. 7 from the Microcalorimetry Research Center.

(1) University of Illinois.
(2) Osaka University.
(3) University of Louisville.
(4) University of Delaware.
(5) University of California at San Diego.

(6) (a) Dong, T.-Y.; Cohn, M. J.; Hendrickson, D. N.; Pierpont, C. G. *J. Am. Chem. Soc.* **1985**, *107*, 4777. (b) Cohn, M. J.; Dong, T.-Y.; Hendrickson, D. N.; Geib, S. J.; Rheingold, A. L. *J. Chem. Soc., Chem. Commun.* **1985**, 1095. (c) Dong, T.-Y.; Hendrickson, D. N.; Iwai, K.; Cohn, M. J.; Rheingold, A. L.; Sano, H.; Motoyama, I.; Nakashima, S. *J. Am. Chem. Soc.* **1985**, *107*, 7996. (d) Dong, T.-Y.; Hendrickson, D. N.; Pierpont, C. G.; Moore, M. F. *J. Am. Chem. Soc.* **1986**, *108*, 963. (e) Moore, M. F.; Wilson, S. R.; Cohn, M. J.; Dong, T.-Y.; Mueller-Westerhoff, U. T.; Hendrickson, D. N. *Inorg. Chem.* **1985**, *24*, 4559. (f) Dong, T.-Y.; Kambara, T.; Hendrickson, D. N. *J. Am. Chem. Soc.* **1986**, *108*, 4423. (g) Dong, T.-Y.; Kambara, T.; Hendrickson, D. N. *J. Am. Chem. Soc.* **1986**, *108*, 5857. (h) Kambara, T.; Hendrickson, D. N.; Dong, T.-Y.; Cohn, M. J. *J. Chem. Phys.* **1987**, *86*, 2362.

0020-1669/90/1329-3547$02.50/0

Several different strategies have been tried in order to delineate the factors that control valence detrapping in $[Fe^{III}_2Fe^{II}O(O_2CCH_3)_6(L)_3]S$ complexes. Changing L from pyridine to various substituted pyridines has been found[7e,f] to change the crystalline packing arrangement. This leads to a dramatic change in the temperature at which valence detrapping occurs. In a series of isostructural Fe_3O complexes with the same ligand L even a change in the solvate molecule S has pronounced effects.[7a,d] The weak (10–100 cm^{-1}) van der Waals interaction between a solvate molecule S and an Fe_3O complex modifies the ground-state potential-energy surface of the Fe_3O complex enough to affect the rate of tunneling of the complex from one minimum to another. This sensitivity to environment reflects the fact that these Fe_3O complexes are electronically labile due to vibronic interactions.[9] It must be emphasized that these $Fe^{III}_2Fe^{II}$ complexes do *not* become electronically delocalized as the temperature is increased, for IR data[10] show they always have a potential-energy barrier.

Two other approaches have been used to characterize the factors controlling intramolecular electron transfer in mixed-valence Fe_3O complexes. It is relatively easy to change the metal. In contrast to the isostructural iron complex, $[Mn_3O(O_2CCH_3)_6(py)_3](py)$ has been reported[11] to valence detrap abruptly in a first-order phase transition occurring in a narrow temperature region around 184.65 K. $[Fe_3O(O_2CCH_3)_6(py)_3](py)$ exhibits two phase transitions, a first-order one at ~112 K, which involves a conversion of valence-trapped complexes from a ferrodistortive alignment to an antiferrodistortive alignment, and a higher-order phase transition, which starts at 115 K and culminates at ~190 K.[7h] This second transition involves both the Fe_3O complexes valence detrapping as well as the onset of motion of the pyridine solvate molecules. Finally, it has been shown[12] very recently with the diamond-anvil ^{57}Fe Mössbauer technique that $[Fe_3O(O_2CCH_3)_6(py)_3](py)$ can be converted at 298 K from valence detrapped to valence trapped upon application of ~83 kbar of pressure. In fact, this complex converts from the paradistortive detrapped phase to the antiferrodistortive phase at ~35 kbar and then to the totally trapped ferrodistortive phase at ~83 kbar.

In the present paper the effects of quenched disorder on the phase transitions of $[Fe_3O(O_2CCH_3)_6(py)_3](py)$ are investigated. This mixed-valence Fe_3O complex is cocrystallized with isostructural $[Fe^{III}_2Co^{II}O(O_2CCH_3)_6(py)_3](py)$ to form the solid solutions $[Fe^{III}_2Fe^{II}_{1-x}Co^{II}_xO(O_2CCH_3)_6(py)_3](py)$. Obviously, each $Fe^{III}_2Co^{II}$ complex is distorted in a direction uniquely determined by the position of the Co^{II} ion. This complex cannot interconvert between different states in the manner the $Fe^{III}_2Fe^{II}$ complex interconverts between its three or four vibronic states. The solid solution contains a kind of quenched disorder. If the $Fe^{III}_2Co^{II}$ complexes behaves as simple impurities, then percolation theory[13] could be used to predict a percolation threshold, that is, a value of x above which only disordered phases of the crystal would exist. The minimum amount (x_c) of *simple* $Fe^{III}_2Co^{II}$ dilutant to breakdown connectivity between domains of $Fe^{III}_2Fe^{II}$ complexes and prevent the formation of the ferrodistortive phase is the percolation threshold. However, each $Fe^{III}_2Co^{II}$ complex is *not* a simple impurity (ie., inactive), for there are py···py intermolecular interactions between each $Fe^{III}_2Co^{II}$ complex and its six neighboring complexes. These intermolecular interactions depend on the sense of distortion of each complex and, consequently, the $Fe^{III}_2Co^{II}$ complex is not an inactive impurity and may at lower concentrations than x_c destroy ordering in the solid solution. Adachi, Panson, and Stratt[14] very recently reported the results of theoretical models devised to examine the effects of this unusual type of quenched disorder on the phase transitions of $[Fe^{III}_2Fe^{II}_{1-x}Co^{II}_xO(O_2CCH_3)_6(py)_3](py)$. They predicted that as x is increased there should be anomalously long relaxation times and a critical $Fe^{III}_2Co^{II}$ impurity concentration that is *not* determined by percolation theory. Heat capacity, ^{57}Fe Mössbauer, and solid-state ^2H NMR data are presented to examine the quenched disorder in this solid solution.

Experimental Section

Compound Preparation. Pyridine was dried by refluxing over BaO and fractionally distilled under an argon atmosphere. The deuterated chemical, pyridine-d_5 (99.5 atm % D), was purchased from Aldrich Chemical Co. and used without further purification. Purified solvents and dried compounds were always stored and manipulated under an argon atmosphere. $[Fe_3O(O_2CCH_3)_6(py)_3](py)$ was prepared by a previously described method.[7h]

$[Fe_2CoO(O_2CCH_3)_6(H_2O)_3]$. Samples of this compound were prepared by a modified method of Weinland and Holtmeier.[15] An 8.08-g (0.02-mol) sample of $Fe(NO_3)_3 \cdot 9H_2O$, 2.91 g (0.01 mol) of $Co(NO_3)_2 \cdot 6H_2O$, and 16.5 g (0.20 mol) of anhydrous sodium acetate were dissolved in 60 mL of distilled water, and the mixture was stirred for 1 day at room temperature. The resulting precipitate was filtered out, washed with 30 mL of ethanol and 30 mL of ethyl ether, and then dried under vacuum for 3 days. The yield was 60–70%.

$[Fe_2CoO(O_2CCH_3)_6(py)_3](py)$. This mixed-metal complex was prepared by dissolving 2 g (3.35 mmol) of $[Fe_2CoO(O_2CCH_3)_6(H_2O)_3]$ in 40 mL of pyridine at 60–70 °C for 1 h, after which impurities were filtered off. The filtrate was allowed to evaporate for 3–4 days in a glovebox. The brownish black crystalline product was filtered out and dried under vacuum. The yield was 1.64 g (57%). Anal. Calcd for $C_{32}H_{38}N_4Fe_2CoO_{13}$: C, 44.83; H, 4.57; N, 6.54; Fe, 13.03; Co, 6.87. Found: C, 44.94; H, 4.51; N, 6.57; Fe, 13.02; Co, 6.95. Crystalline samples of $[Fe_2CoO(O_2CCH_3)_6(C_5D_5N)_3](C_5D_5N)$ were prepared by the same method with deuterated pyridine.

$[Fe^{III}_2Fe^{II}_{0.5}Co^{II}_{0.5}O(O_2CCH_3)_6(py)_3](py)$. Samples of this solid-solution complex were prepared by cocrystallization with appropriate amounts of the $[Fe_3O(O_2CCH_3)_6(py)_3](py)$ and $[Fe_2CoO(O_2CCH_3)_6(py)_3](py)$ based on the weight ratio. Anal. Calcd for $C_{32}H_{38}H_4Fe_{2.5}Co_{0.5}O_{13}$: C, 44.91; H, 4.48; N, 6.55; Fe, 16.32; Co, 3.44. Found: C, 44.60; H, 4.44; N, 6.60; Fe 16.45; Co, 3.52.

Physical Measurements. Variable-Temperature ^{57}Fe Mössbauer Spectroscopy. Variable-temperature Mössbauer spectra were obtained in vertical transmission geometry by using a constant-acceleration spectrometer that has been described before.[16] The sample temperature, controlled by a Lake Shore Cryotronics Model DRC80C temperature controller in conjunction with a silicon diode mounted on the copper sample cell holder, is estimated to have an absolute accuracy of ±3 K. Computer fittings of the Mössbauer data to Lorentzian line shapes were carried out with a modified version of a previously reported computer program.[17] The isomer shift values are reported relative to iron foil at 298 K but are not corrected for the temperature-dependent second-order doppler shift.

(7) (a) Jang, H. G.; Geib, S. J.; Kaneko, Y.; Nakano, M.; Sorai, M.; Rheingold, A. L.; Montez, B.; Hendrickson, D. N. *J. Am. Chem. Soc.* **1989**, *111*, 173. (b) Kaneko, Y.; Nakano, M.; Sorai, M.; Jang, H. G.; Hendrickson, D. N. *Inorg. Chem.* **1989**, *28*, 1067. (c) Oh, S. M.; Wilson, S. R.; Hendrickson, D. N.; Woehler, S. E.; Wittebort, R. J.; Inniss, D.; Strouse, C. E. *J. Am. Chem. Soc.* **1987**, *109*, 1073. (d) Woehler, S. E.; Wittebort, R. J.; Oh, S. M.; Kambara, T.; Hendrickson, D. N.; Inniss, D.; Strouse, C. E. *J. Am. Chem. Soc.* **1987**, *109*, 1063. (e) Woehler, S. E.; Wittebort, R. J.; Oh, S. M.; Hendrickson, D. N.; Inniss, D.; Strouse, C. E. *J. Am. Chem. Soc.* **1986**, *108*, 2938. (f) Hendrickson, D. N.; Oh, S. M.; Dong, T.-Y.; Kambara, T.; Cohn, M. J.; Moore, M. F. *Comments Inorg. Chem.* **1985**, *4*, 329. (g) Sorai, M.; Shiomi, Y.; Hendrickson, D. N.; Oh, S. M.; Kambara, T. *Inorg. Chem.* **1987**, *26*, 223. (h) Sorai, M.; Kaji, K.; Hendrickson, D. N.; Oh, S. M. *J. Am. Chem. Soc.* **1986**, *108*, 702.

(8) Sorai, M.; Nishimori, A.; Hendrickson, D. N.; Dong, T.-Y.; Cohn, M. J. *J. Am. Chem. Soc.* **1987**, *109*, 4266.

(9) Bersuker, I. B. *The Jahn-Teller Effect and Vibronic Interactions in Modern Chemistry*; Plenum Press: New York, 1984.

(10) (a) Cannon, R. D.; White, R. P. *Prog. Inorg. Chem.* **1988**, *36*, 195. (b) Cannon, R. D.; Montri, L.; Brown, D. B.; Marshall, K. M.; Elliott, C. M. *J. Am. Chem. Soc.* **1984**, *106*, 2591.

(11) (a) Jang, H. G.; Vincent, J. B.; Nakano, M.; Huffman, J. C.; Christou, G.; Sorai, M.; Wittebort, R. J.; Hendrickson, D. N. *J. Am. Chem. Soc.* **1989**, *111*, 7778. (b) Nakano, M.; Sorai, M.; Vincent, J. B.; Christou, G.; Jang, H. G.; Hendrickson, D. N. *Inorg. Chem.* **1989**, *28*, 4608–4614.

(12) McCusker, J. K.; Jang, H. G.; Zvagulis, M.; Ley, W.; Drickamer, H. G.; Hendrickson, D. N. Submitted for publication.

(13) (a) Efros, A. L. *Physics and Geometry of Disorder, Percolation Theory*; Mir Publishers: Moscow, 1986. (b) Stinchcombe, R. B. In *Phase Transitions*; Dombe, C., Lebowitz, J. L., Eds.; Academic Press: New York, 1983; Vol. 7, Chapter 3.

(14) Adachi, S. H.; Panson, A. E.; Stratt, R. M. *J. Chem. Phys.* **1988**, *88*, 1134.

(15) Weinland, R.; Holtmeier, H. *Z. Anorg. Chem.* **1928**, *173*, 49.

(16) Cohn, M. J.; Timken, M. D.; Hendrickson, D. N. *J. Am. Chem. Soc.* **1984**, *106*, 6683.

(17) Chrisman, B. L.; Tumolillo, T. A. *Comput. Phys. Commun.* **1971**, *2*, 322.

Table I. Crystallographic Data for $[Fe_3O(O_2CCH_3)_6(py)_3](py)$ (**1**) and $[Fe_2CoO(O_2CCH_3)_6(py)_3](py)$ (**2**)

compd	complex **1**	complex **2**
formula	$C_{32}H_{38}Fe_3N_4O_{12}$	$C_{32}H_{38}CoFe_2N_4O_{12}$
fw	838.16	841.24
cryst system	rhombohedral	rhombohedral
space group	$R32$	$R32$
a, Å	17.558 (7)[a]	17.583 (6)
c, Å	11.074 (4)	11.074 (3)
V, Å^3	2963.3 (7)	2965.0 (6)
Z	3	3
μ, cm^{-1}	11.8	12.4
d(calcd), g/cm^3	1.409	1.413
temp, °C	25	25
radiation; λ, Å	Mo Kα; 0.7107	Mo Kα; 0.7107
R_F, %	3.17	3.72
R_{wF}, %	3.48	4.05

[a] Unit cell parameters were obtained from the angular settings of 25 reflections ($22° \le 2\theta \le 30°$) containing Friedel pairs to monitor optical and mechanical alignment.

Solid-State ^{2}H NMR Spectroscopy. ^{2}H NMR experiments were performed on a homebuilt 5.9-T spectrometer described elsewhere[18] with the solid echo pulse sequence $[(90)_x$-$t/2$-$(90)_y$-$t/2$-observe]. A value of $t = 50$ μs and a 90° pulse width of 2.5 μs were used. NMR samples consisted of ~50 mg of tightly or loosely packed microcrystals sealed into a Delrin tube ($^1/_4 \times {}^1/_4 \times {}^1/_2$ in). In the case of the random powder spectra, the sample was prepared by mixing the microcrystals in the fluid eicosane hydrocarbon matrix outside the magnetic field and then it was cooled to room temperature. For the magnetically oriented microcrystalline sample, a stream of dry nitrogen gas at 50 °C was passed over the hydrogen matrix melting the eicosane and then the microcrystals were oriented by the 5.9-T magnetic field such that the principal axis of the magnetic susceptibility tensor of each microcrystal was aligned with external magnetic field. The hydrocarbon was then cooled to form a block with the microcrystals embedded in it. The hydrocarbon block was mounted about a single axis perpendicular to the magnetic field.

Heat Capacity Measurements. Heat capacities were measured with an adiabatic calorimeter.[19] A calorimeter cell made of gold-plated copper was loaded with 16.6562 g (0.0159580 mol) of $[Fe^{III}_2Fe^{II}_{0.5}Co^{II}_{0.5}O(O_2CCH_3)_6(py)_3](py)$ and 17.4981 g (0.0204107 mol) of $[Fe_2CoO(O_2CCH_3)_6(py)_3](py)$ with buoyancy correction assuming the density of 1.4 g cm^{-3}. A small amount of helium gas was sealed in the cell to aid heat transfer.

Crystal Measurements, Data Collection, and X-ray Structure Refinement for $[Fe_3O(O_2CCH_3)_6(py)_3](py)$ (1) and $[Fe_2CoO(O_2CCH_3)_6(py)_3](py)$ (2). Crystallographic data are collected in Table I. Deep red crystals of **1** and **2** were mounted on glass fibers and found to be isomorphous with the previously reported 200 K structure of **1**.[7e] Corrections for absorption were applied to both data sets (empirical, four-scan, 216 data, six reflections each).

Heavy-atom positions were initialized from those reported in ref 7e. In **2**, the mixed Fe/Co site ($^2/_3$ Fe, $^1/_3$ Co) was refined as a Co atom with a site-occupany-factor of 0.975. Both lattices contain a molecule of pyridine of solvation for each trimetal complex. The py molecule is disordered in three sites about the 3-fold axis centered at 32-symmetry sites such that the plane of each molecule is perpendicular to the 2-fold axis and parallel to the 3-fold axis. The two unique atoms that form the three py sites are labeled X(1) and X(2) with X(1) fixed at $^2/_3$ occupancy and X(2) at $^1/_3$ occupancy. It was not possible to determine the carbon versus nitrogen character of these sites, and both were treated as carbon atoms.

All non-hydrogen atoms except for X(1) and X(2) were anisotropically refined. Hydrogen atoms for the methyl group and the coordinated py molecule were treated as fixed, idealized contributions. The hydrogen atoms of the disordered solvent molecule were ignored.

All computations and sources of scattering factors used the SHELXTL (5.1) library (G. Sheldrick, Nicolet XRD, Madison, WI).

Results and Discussion

Single-Crystal X-ray Structures of $[Fe_3O(O_2CCH_3)_6(py)_3](py)$ (1) and $[Fe_2CoO(O_2CCH_3)_6(py)_3](py)$ (2). The molecule and solid-state structures of **1** and **2** have been determined at 298 K. Both complexes crystallize in the space group $R32$ with $Z = 3$.

Table II. Positional Parameters for $[Fe_3O(O_2CCH_3)_6(py)_3](py)$ (**1**)

atom	x/a	y/b	z/c
Fe	0.8913 (1)	0.8913 (1)	0.5000
O(1)	1.0000	1.0000	0.5000
O(2)	0.9248 (2)	0.8325 (2)	0.3664 (3)
O(3)	0.8311 (2)	0.9294 (2)	0.3716 (3)
N	0.7646 (2)	0.7646 (2)	0.5000
C(1)	0.9973 (2)	0.8440 (2)	0.3336 (4)
C(2)	0.9968 (3)	0.7825 (3)	0.2387 (4)
C(3)	0.6891 (2)	0.7626 (3)	0.4866 (4)
C(4)	0.6087 (3)	0.6848 (3)	0.4832 (4)
C(5)	0.6077 (3)	0.6077 (3)	0.5000
X(1)[a]	0.9558 (11)	0.9633 (9)	0.9021 (10)
X(2)	0.9301 (14)	0.9301 (14)	1.0000 (8)

[a] X(1) and X(2) compose the disordered pyridine solvent molecules (see Experimental Section).

Table III. Positional Parameters for $[Fe_2CoO(O_2CCH_3)_6(py)_3](py)$ (**2**)

atom	x/a	y/b	z/c
Fe(Co)	0.8914 (1)	0.8914 (1)	0.5000
O(1)	1.0000	1.0000	0.5000
O(2)	0.9019 (2)	1.0705 (2)	0.6277 (3)
O(3)	0.8331 (2)	0.9244 (2)	0.6338 (2)
N(1)	0.7659 (2)	0.7658 (2)	0.5000
C(1)	0.8447 (2)	0.9975 (2)	0.6657 (4)
C(2)	0.7823 (3)	0.9969 (3)	0.7608 (4)
C(3)	0.6897 (2)	0.7630 (3)	0.4863 (4)
C(4)	0.6099 (3)	0.6865 (3)	0.4835 (4)
C(5)	0.6090 (3)	0.6090 (3)	0.5000
X(1)[a]	−0.0015 (12)	0.0384 (8)	−0.1064 (11)
X(2)	0.0000	0.0769 (19)	0.0000

[a] X(1) and X(2) composed the disordered pyridine solvent molecule (see Experimental Section).

Table IV. Selected Bond Distances and Angles of the Central Atoms for $[Fe_3O(O_2CCH_3)_6(py)_3](py)$ (**1**) at 297 K

Bond Distances (Å)			
Fe–O(1)	1.910 (1)	C(1)–O(3)	1.247 (4)
Fe–O(1)	2.053 (3)	C(1)–C(2)	1.505 (8)
Fe–O(3)	2.074 (3)	C(3)–N(1)	1.319 (5)
Fe–N(1)	2.228 (4)	C(3)–C(4)	1.391 (5)
C(1)–O(2)	1.241 (5)	C(4)–C(5)	1.359 (7)
Bond Angles (deg)			
Fe–O(1)–Fe	120.0	O(2)–Fe–O(3)	89.4 (1)
O(1)–Fe–N(1)	180.0	O(2)–Fe–N(1)	83.8 (1)
O(1)–Fe–O(2)	96.2 (1)	O(3)–Fe–N(1)	84.6 (1)
O(1)–Fe–O(3)	95.4 (1)		

Previously we reported[7e] the structure of complex **1** at 200 K where it still has the $R32$ symmetry. Below ~190 K where the higher order phase transition culminates it was not possible to determine the X-ray structure of complex **1**, for each diffraction peak reversibly splits into several peaks due to internal twinning (domain structure). However, we did show that below ~190 K the crystallographic C_3 axis disappears.

Details of the X-ray diffraction measurements and refinement for complexes **1** and **2** at 298 K are given in Table I. Drawings of the molecular structures of **1** and **2** are shown in Figure 1. In both cases the triply bridging oxygen atom resides at a site of 32 symmetry. The central O^{2-} ion, the three metal atoms, and the three pyridine nitrogen atoms lie exactly in the plane. Obviously, in the case of the $Fe^{III}_2Co^{II}$ complex **2** there is a static disorder of the three metal atoms. Atomic coordinates for complexes **1** and **2** are given in Tables II and III, respectively.

As found for complex **1** at 298 K, the Fe(Co)–O(oxide) distance [1.910 (1) Å] in complex **2** is equal to the average of two times the Fe^{III}–O [1.862 (4) Å] and one times the Fe^{II}–O distance [2.006 (4) Å] found[20] for the toluene solvate $[Fe_3O(O_2CCH_3)_6(3\text{-Et-py})_3]\cdot{}^1/_2C_6H_5CH_3$ at 298 K, a complex that is known[20] to be

(18) Wittebort, R. J.; Subramanian, R.; Kulshreshtha, N. P.; Du Pre, D. B. *J. Chem. Phys.* **1985**, *83*, 2457.
(19) Sorai, M.; Kaji, K. Construction of an adiabatic calorimeter capable of measuring heat capacities between 12 and 530 K (unpublished).
(20) Jang, H. G.; Thean, J. M.; Geib, S. J.; Rheingold, A. L.; Hendrickson, D. N. Manuscript in preparation.

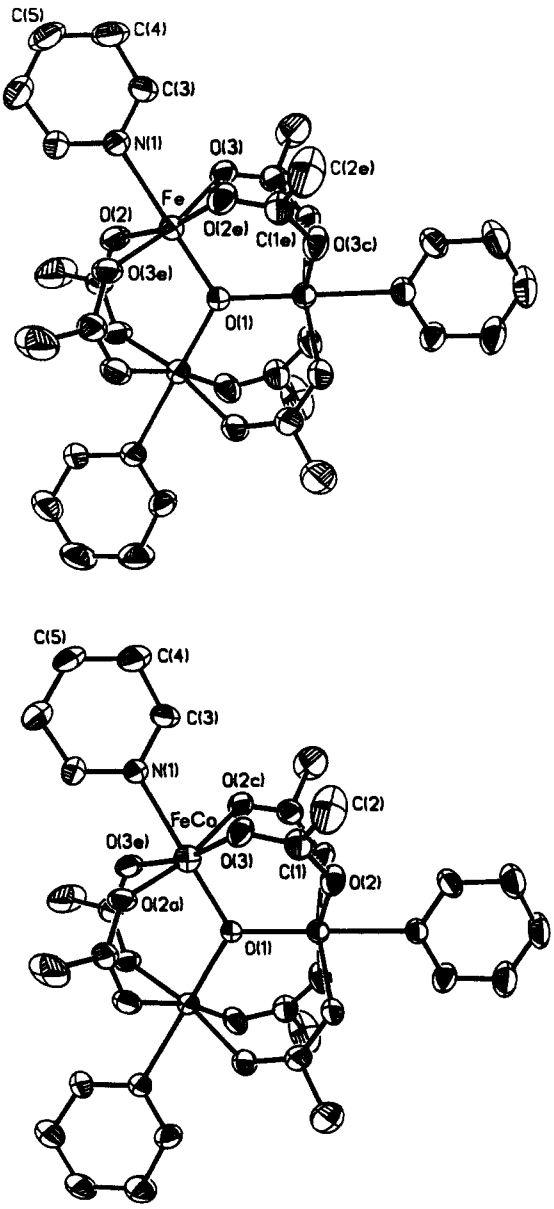

Figure 1. ORTEP plots of the molecular structures at 298 K of the μ_3-oxo-bridged trinuclear complexes in $[Fe_3O(O_2CCH_3)_6(py)_3](py)$ (**1**) and $[Fe_2CoO(O_2CCH_3)_6(py)_3](py)$ (**2**). Atoms are shown as 50% equiprobability ellipsoids.

Table V. Selected Bond Distances and Angles of the Central Atoms for $[Fe_2CoO(O_2CCH_3)_6(py)_3](py)$ (**2**) at 297 K

Bond Distances (Å)			
Fe(Co)-O(1)	1.909 (1)	C(1)-O(3)	1.249 (4)
Fe(Co)-O(2)	2.065 (3)	C(1)-C(2)	1.517 (8)
Fe(Co)-O(3)	2.043 (3)	C(3)-N(1)	1.324 (5)
Fe(Co)-N(1)	2.208 (4)	C(3)-C(4)	1.375 (5)
C(1)-O(2)	1.242 (4)	C(4)-C(5)	1.367 (7)
Bond Angles (deg)			
Fe-O(1)-Co	120.0	O(2)-Fe(Co)-O(3)	89.7 (1)
O(1)-Fe(Co)-N(1)	180.0	O(2)-Fe(Co)-N(1)	84.7 (1)
O(1)-F(Co)-O(2)	95.3 (1)	O(3)-Fe(Co)-N(1)	83.7 (1)
O(1)-Fe(Co)-O(3)	96.3 (1)		

valence trapped not only at low temperatures but also at 350 K. In Tables IV and V, respectively, are given bond distances and angles of the central atoms for complexes **1** and **2**. There does not appear to be any appreciable differences in metric details for these two complexes.

As viewed down the *c* axis, the crystal packing arrangement for the Fe_3O complex **1** is shown in Figure 2. The same packing arrangement is obviously present for **2**. Along the *c* axis Fe_2MO (M = Fe, Co) complexes and pyridine solvate molecules occupy

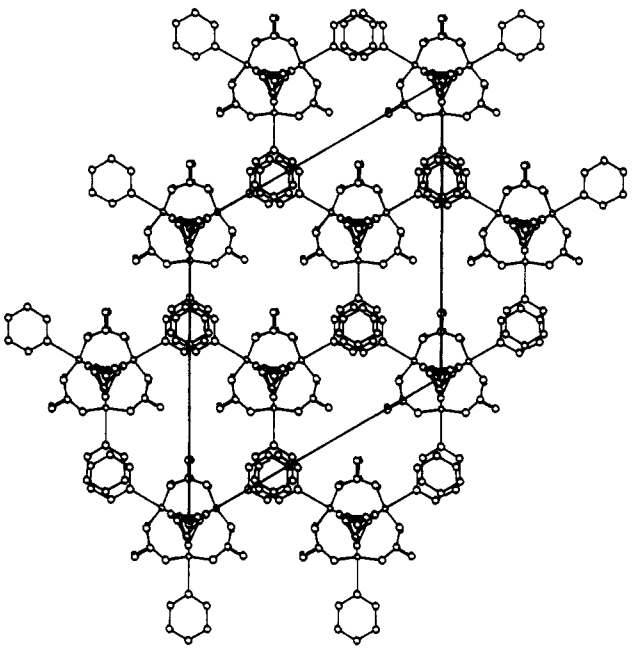

Figure 2. ORTEP view of the stacking of trinuclear complexes and pyridine solvate molecules along the crystallographic *c* axis for $[Fe_3O(O_2CCH_3)_6(py)_3](py)$ (**1**). Each pyridine solvate molecule is aligned along the stacking direction with its ring plane parallel to the *c* axis and disordered in three positions.

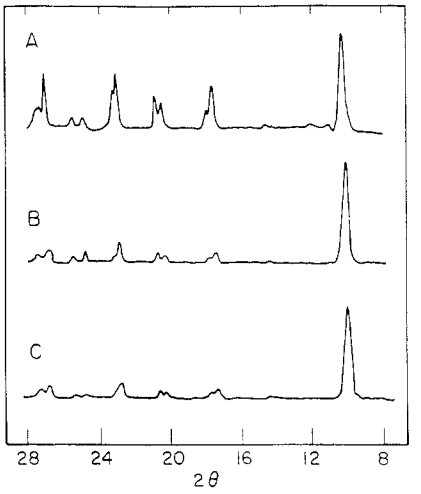

Figure 3. Room-temperature powder X-ray diffraction patterns: (A) $[Fe_3O(O_2CCH_3)_6(py)_3](py)$; (B) $[Fe^{III}_2Fe^{II}_{0.5}Co^{II}_{0.5}O(O_2CCH_3)_6(py)_3](py)$; (C) $[Fe^{III}_2CoO(O_2CCH_3)_6(py)_3](py)$.

alternating sites of 32 symmetry. Each pyridine solvate molecule is sandwiched between two Fe_2MO complexes. The plane of the pyridine solvate molecule is perpendicular to the Fe_2MO plane. Furthermore, each pyridine solvate molecule is 3-fold disordered about the crystallographic C_3 axis, ie., the *c* axis.

In addition to the contacts between pyridine solvate and Fe_2MO molecules, another significant intermolecular interaction exists between pyridine ligands of Fe_2MO molecules in adjacent stacks. The interplanar distance between these py···py contacts is $c/3$, which is 3.690 Å for both complexes **1** and **2**. There is a small difference in *a* and *b* unit cell parameters (Table I). The py···py contact is slipped more for complex **2**, and thus, this interaction is weaker for complex **2** than for complex **1**. Tables of detailed bond lengths and angles, anisotropic thermal parameters, and hydrogen atom coordinates and listings of structure factor amplitudes for complexes **1** and **2** are available in the supplementary material.

In Figure 3 are shown the room-temperature powder X-ray diffraction patterns for complexes **1** and **2** and for $[Fe^{III}_2Fe^{II}_{0.5}Co^{II}_{0.5}O(O_2CCH_3)_6(py)_3](py)$ (**3**). It is not surprising the solid solution **3** also has $R32$ symmetry. However, the data

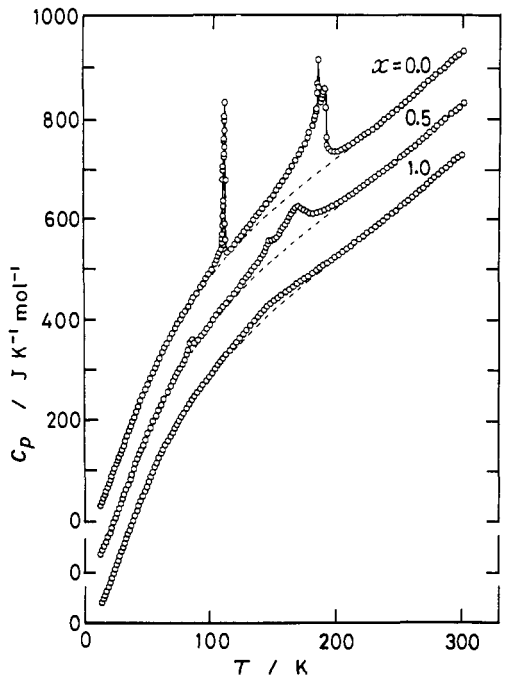

Figure 4. Plots of molar heat capacity at constant pressure, C_P, versus temperature for three complexes of the composition $[Fe^{III}_2Fe^{II}_{1-x}Co^{II}_xO(O_2CCH_3)_6(py)_3](py)$. Complex **1** with $x = 0$ is the undoped Fe_3O complex, complex **2** with $x = 1.0$ is the undoped $Fe^{III}_2Co^{II}O$ complex, and complex **3** is the 50% solid solution where $x = 0.5$. Broken curves indicate the normal heat capacities.

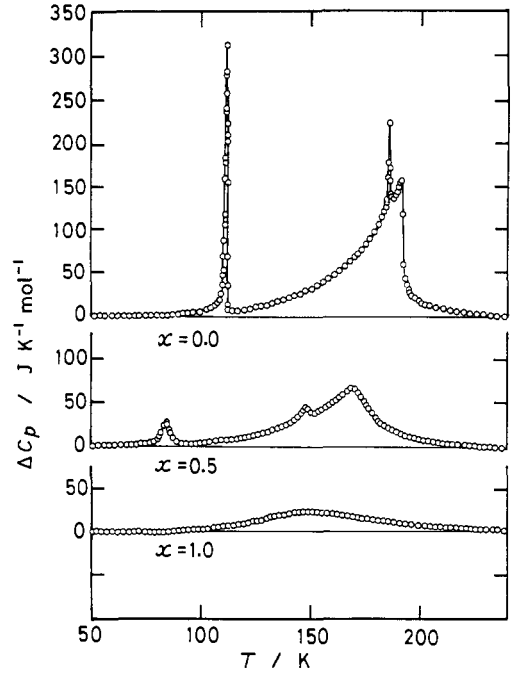

Figure 5. Plots of the excess heat capacity at constant pressure, ΔC_P, versus temperature for the three complexes of the composition $[Fe^{III}_2Fe^{II}_{1-x}Co^{II}_xO(O_2CCH_3)_6(py)_3](py)$.

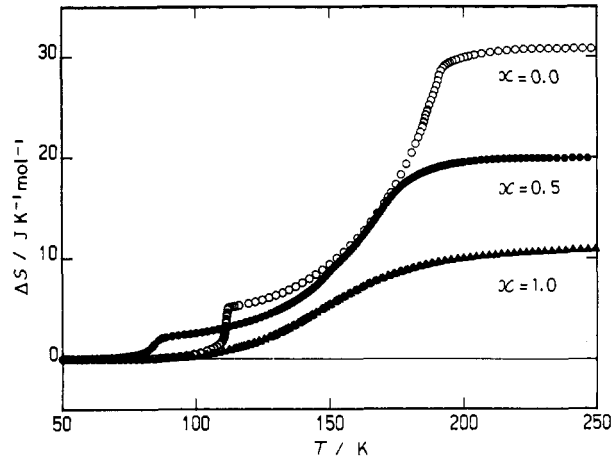

Figure 6. Plots of the total transition entropy, ΔS, versus temperature for the three complexes of the composition $[Fe^{III}_2Fe^{II}_{1-x}Co^{II}_xO(O_2CCH_3)_6(py)_3](py)$.

in Figure 3 are crucial for they show that compound **3** is indeed a solid solution, not just a mixture of crystals of **1** and **2**. This is indicated by the fact that the main powder XRD peaks for **3** fall at 2θ values different from those of the peaks for **1** and **2**. In fact, the peak positions for **3** are intermediate between the corresponding peaks for **1** and **2**. It is important for the discussion of this paper that statistically distributed solid solutions of the Fe_3O and Fe_2CoO complexes form.

Heat Capacity Measurements. Heat capacity data for $[Fe_3O(O_2CCH_3)_6(py)_3](py)$, obtained in an adiabatic calorimeter, were reported[7h] in detail previously in the range of 12–300 K. The plot of heat capacity at constant pressure, C_P, versus temperature for complex **1** is reproduced in Figure 4, where it can be seen that complex **1** exhibits basically two phase transitions. A first-order phase transition with two sharp C_P peaks at 111.4 and 112.0 K is seen, together with a higher order phase transition that starts from ~113 K to culminate in two C_P peaks at 185.8 and 191.5 K. The total enthalpy and entropy of these phase transitions were determined to be $\Delta H = 4940$ J mol^{-1} and $\Delta S = (30.58 \pm 0.83)$ J K^{-1} mol^{-1}, respectively.

In the present study, the heat capacity at constant pressure was measured in the 12–300 K range for a 17.4981-g sample of $[Fe_2CoO(O_2CCH_3)_6(py)_3](py)$ (**2**) and a 13.6562-g sample of $[Fe^{III}_2Fe^{II}_{0.5}Co^{II}_{0.5}O(O_2CCH_3)_6(py)_3](py)$ (**3**). The molar heat capacities of compounds **2** and **3** are plotted in Figure 4. Relative to the case of the $Fe^{III}_2Fe^{II}$ complex **1**, the C_P data for the solid solution complex **3** show that all the phase transitions for **3** are shifted to lower temperatures and the heat capacity peaks become broader. For complex **3**, C_P peaks are seen at 84.5, 148.0, and 168.8 K. These peak positions are in agreement with those 86.3, 151.8, and 172.2 K reported[7h] from DTA heating runs of the same $x = 0.5$ solid-solution compound.

As can be seen in Figure 4, there is only one very broad C_P peak seen at 148.5 K for the $Fe^{III}_2Co^{II}$ complex **2**. It can be anticipated (vide infra) that this broad peak is attributable only to the onset of motion of the pyridine solvent molecules, for the $Fe^{III}_2Co^{II}$ molecules in **2** must remain trapped in one distorted state.

An effective frequency-distribution method[21] was employed to estimate a normal lattice heat capacity curve. The difference between the observed and normal heat capacities is the excess heat capacity, ΔC_P, due to phase transitions. In Figure 5 are given plots of ΔC_P versus temperature for complexes **2** and **3**, and for comparison the data reported for complex **1** are also plotted. As can be seen in Figure 5, the main valence-detrapping phase transition for the solid solution **3**, which for complex **1** starts at ~113 K and culminates fairly abruptly at ~190 K, not only is shifted to lower temperature (peak at 169 K) but also becomes very broadened. For the solid solution **3** ΔC_P begins to appear at ~100 K for the valence-detrapping phase transition, there is a maximum in ΔC_P at 169 K, and however, there is considerable excess heat capacity up to ~230 K.

In the case of $Fe^{III}_2Co^{II}$ complex **2** the ΔC_P versus temperature plot shows one broad feature starting at ~100 K and continuing to ~230 K with a maximum at 149 K. There is no evidence of the low-temperature phase transition for complex **2**.

Integration of the ΔC_P versus temperature data for complexes **2** and **3** with respect to T and ln T gave the total enthalpy change (ΔH) and entropy change (ΔS), respectively, arising from the phase transitions in these two compounds. For complex **2** we obtained $\Delta H = 1550$ J mol^{-1} and $\Delta S = 10.32$ J K^{-1} mol^{-1}, whereas, for the solid-solution complex **3**, $\Delta H = 2910$ J mol^{-1} and $\Delta S =$

(21) Sorai, M.; Seki, S. *J. Phys. Soc. Jpn.* **1972**, *32*, 382.

Table VI. ^{57}Fe Mössbauer Fitting Parameters for $[Fe^{III}_2Fe^{II}_{0.5}Co^{II}_{0.5}O(O_2CCH_3)_6(py)_3](py)$[a]

	δ, mm/s[b]			ΔE_Q, mm/s			Γ, mm/s[c]			% area		
T, K	Fe^{III}	Fe^{av}	Fe^{II}	Fe^{III}	Fe^{av}	Fe^{II}	Fe^{III}	Fe^{av}	Fe^{II}	Fe^{III}	Fe^{av}	Fe^{II}
85	0.526 (1)		1.260 (4)	1.121 (1)		1.778 (8)	0.177 (1)		0.240 (8)	80.0 (1)		20.0 (1)
							0.177 (1)		0.268 (6)			
95	0.526 (1)	0.728 (9)	1.161 (1)	1.120 (1)	0.543 (1)	1.778 (9)	0.162 (1)	0.255 (2)	0.247 (2)	69.0 (2)	14.2 (2)	16.8 (1)
							0.162 (1)	0.255 (2)	0.247 (2)			
120	0.520 (1)	0.775 (9)	1.092 (2)	1.107 (2)	0.474 (1)	1.671 (1)	0.167 (2)	0.276 (2)	0.221 (2)	64.8 (1)	26.0 (1)	9.2 (1)
							0.167 (2)	0.276 (2)	0.221 (2)			
140	0.515 (2)	0.784 (2)	0.962 (2)	1.104 (3)	0.470 (7)	1.508 (9)	0.164 (2)	0.310 (2)	0.072 (9)	59.0 (2)	38.4 (2)	2.6 (2)
							0.164 (2)	0.310 (2)	0.072 (9)			
200	0.493 (7)	0.754 (3)		1.117 (3)	0.452 (2)		0.152 (2)	0.231 (6)		51.8 (2)	48.2 (2)	
							0.152 (2)	0.231 (6)				
220	0.493 (6)	0.748 (3)		1.122 (3)	0.486 (2)		0.150 (2)	0.225 (4)		51.8 (2)	48.2 (2)	
							0.150 (2)	0.225 (0)				
250	0.475 (2)	0.723 (3)		1.105 (4)	0.529 (7)		0.140 (2)	0.189 (4)		51.6 (1)	48.4 (2)	
330	0.464 (3)	0.704 (5)		1.101 (6)	0.607 (7)		0.128 (3)	0.176 (4)		48.0 (2)	52.0 (2)	
							0.128 (3)	0.176 (4)				

[a] Peaks were least-squares fit to Lorentzian line shapes with equal areas for both components of a doublet; error in the last significant figure is given in parentheses. [b] Center shifts relative to Fe metal at room temperature. [c] Half-width at half-maximum listed in order of increasing velocity of the peak.

19.74 J K^{-1} mol^{-1} were calculated. In Figure 6 ΔS versus temperature is plotted for complexes **1–3**. The differences in the temperature dependencies of entropy gain are quite interesting and deserving of comment. However, it is appropriate first to suggest a model for the differences in total entropy gains for complexes **1–3**. In our previous papers[7d,h] it was concluded that when complex **1** is heated from low temperatures, each Fe_3O complex converts from being statically distorted in one state to interconverting dynamically between *three* vibronic states. This contributes R ln 3 to the total entropy gain. Solid-state ^{2}H NMR data also showed that the pyridine solvate molecule in **1** converts from being static to dynamically interconverting among *twelve* different orientations. The plane of the pyridine molecule jumps between three positions about the crystallographic C_3 axis. In each planar position the pyridine solvate molecule librates between four positions where in each of these positions two carbon atoms are on the C_3 axis. The onset of motion of the pyridine solvate molecules contributes R ln 12 to ΔS for complex **1**. The sum of R ln 3 for the Fe_3O constituents and R ln 12 for the solvate molecules gives ΔS = 29.79 J K^{-1} mol^{-1}. This value agrees well with the observed ΔS = (30.58 ± 0.83) J K^{-1} mol^{-1} for **1**.

For $[Fe_2CoO(O_2CCH_3)_6(py)_3](py)$ the total experimental entropy gain is ΔS = 10.32 J K^{-1} mol^{-1}. This value is close to R ln 3 = 9.13 J K^{-1} mol^{-1}. As substantiated by solid-state ^{2}H NMR results (vide infra), the single broad phase transition for Fe_2Co complex **2** involves the onset of dynamics associated with the pyridine solvate molecules jumping between three positions about the C_3 axis. This obviously contributes R ln 3 to the entropy gain. There is no other motion of the pyridine solvate molecules of complex **2** that is occurring cooperatively in the phase transition. At room temperature and temperatures well below the phase transition of **2**, ^{2}H NMR data show that the pyridine solvate molecules are, in addition to jumping about the C_3 axis, rotating in plane about a local pseudo-C_6 axis. This second motion is not coupled to the phase transition.

It is fascinating that the total entropy gain exhibited by $[Fe^{III}_2Fe^{II}_{0.5}Co^{II}_{0.5}O(O_2CCH_3)_6(py)_3](py)$ appears to be close to what one would predict from simple additivities. The experimental value of ΔS = 19.74 J K^{-1} mol^{-1} is predicted by eq 1. Thus, the

$$\Delta S = (1 - x)[R \ln 3 + R \ln 12] + x(R \ln 3) \qquad (1)$$

solid solution **3** comprises a statistical distribution of 50% Fe_3O complexes and 50% Fe_2CoO complexes. The first term in eq 1, i.e., $(1 - x)[R \ln 3 + R \ln 12]$, is an entropy gain reflecting the $(1 - x)$ amount of Fe_3O moelcules, and the second term in eq 1 is an entropy gain reflecting the x amount of Fe_2CoO complexes. When x is taken as 0.5 as for complex **3**, then eq 1 gives ΔS = 19.46 J K^{-1} mol^{-1}. This value is surprisingly close to the experimental value. This additivity of ΔS contributions could be taken to indicate that the crystals of the solid-solution complex **3** are made up of domains (regions) containing either only Fe_3O complexes or only Fe_2CoO complexes. However, this cannot be the case, for the powder XRD patterns (Figure 3) show peaks with 2θ values that are intermediate between those for complexes **1** and **2**. There are *not* domains of Fe_3O or Fe_2CoO complexes large enough to show diffraction peaks. Additional evidence for no domain formation is definitely given by the temperature shift of the phase transitions. If the specimen was made up of domains containing either only Fe_3O complex or only Fe_2CoO complexes, the respective phase transition temperatures for the solid solution **3** would remain at the same values as those for **1** although the heat capacity peaks would be reduced by half for **3**. Obviously this is not the case.

Each pyridine solvate molecule is sandwiched between two Fe_2MO (M = Fe, Co) complexes. When either of its two neighboring Fe_2MO complexes is a Fe_3O complex, the in-plane librational motion of the pyridine solvate molecule apparently is more restricted (ie., not complete rotation about a local pseudo-C_6 axis) than if both neighbors are Fe_2CoO complexes and the restricted librational motion is coupled to the phase transition. This later situation could reflect the fact that it is only the Fe_3O complex that valence detraps and when it is interconverting between its vibronic states, it undergoes large-amplitude vibrational motion.

^{57}Fe Mössbauer Spectroscopy. Variable-temperature Mössbauer spectra were run for Fe_2CoO complex **2** and solid-solution complex **3**. In the case of complex **2**, the spectra show only one quadrupole-split doublet from 120 to 296 K; see Figure 7. This doublet has at 296 K typical values of isomer shift (δ = 0.513 mm/s versus iron foil) and quadrupole splitting (ΔE_Q = 0.904 mm/s) that correspond to those of a high-spin Fe^{III} ion. Clearly, intramolecular electron transfer does not occur in complex **2**.

The Mössbauer spectrum of the solid-solution complex **3** is temperature dependent; see Figure 8. Two quadrupole-split doublets are seen at 85 K; one has parameters (see Table VI) characteristic of high-spin Fe^{III} and the other doublet is that of a high-spin Fe^{II} ion, where the area ratio of the two doublets is 4:1 as expected, for there are two Fe^{III} ions in each Fe_3O complex as well as in each Fe_2CoO complex. The spectra were least-squares fit to Lorentzian line shapes; the resulting parameters are collected in Table VI.

The 95 K spectrum for complex **3** could *not* be fit well to only two doublets. It was necessary to use a third doublet. The fitting parameters for this third doublet are those found for a valence-detrapped complex. In the temperature range between 95 and 140 K the area of this third doublet increases monotonically from 14.2 to 38.4%. Finally, above ~200 K the spectrum comprises only two quadrupole-split doublets, one is characteristic of high-spin Fe^{III} ion and the other doublet is that of a valence-detrapped signal. The former arises from Fe^{III} sites in $Fe^{III}_2Co^{II}O$ complexes, and the latter, from valence-detrapped Fe_3O complexes.

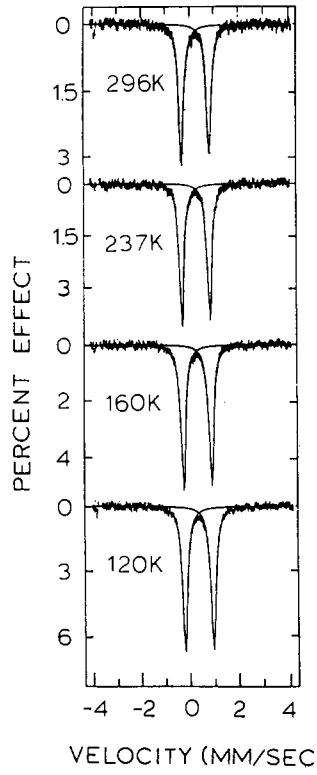

Figure 7. Variable-temperature ^{57}Fe Mössbauer spectra for $[Fe_2CoO(O_2CCH_3)_6(py)_3](py)$ (**2**).

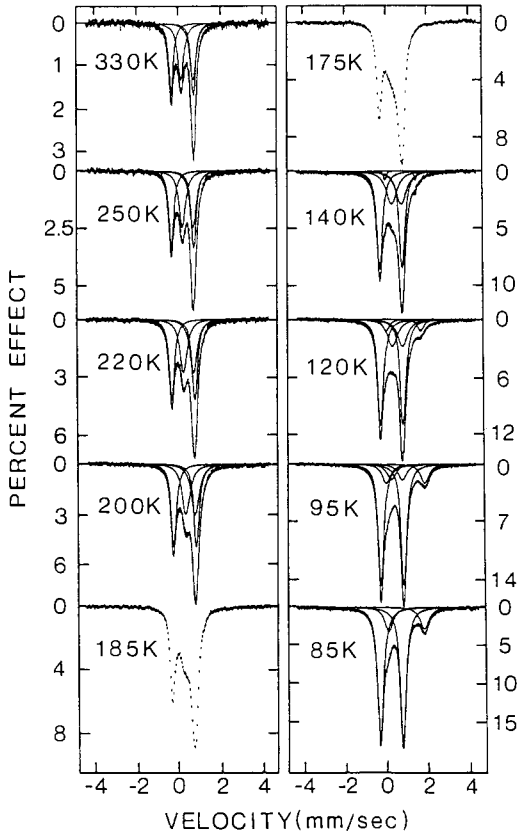

Figure 8. Variable-temperature ^{57}Fe Mössbauer spectra for $[Fe^{III}_2Fe^{II}_{0.5}Co^{II}_{0.5}O(O_2CCH_3)_6(py)_3](py)$.

It is interesting that the area ratio of valence-detrapped doublet to Fe^{III} doublet is 0.930 at 200 and 220 K and increases to 0.938 at 250 K and finally 1.083 at 330 K. The simple expectation would be 1.50 for this ratio, for there are presumably equal amounts of valence-detrapped Fe_3O complexes as well as $Fe^{III}_2Co^{II}O$ complexes in the 200–330 K range. The experimental area ratio is probably less than 1.50 for one reason. In this temperature region each valence-detrapped Fe_3O complex is rapidly interconvering between its three (or four) vibronic states. This happens as a result of the Fe_3O complex undergoing large-amplitude vibrational motion where appreciable dimensional changes are occurring to interconvert between different vibronic states such as, for example, $Fe^{III}_aFe^{III}_bFe^{II}_c$ and $Fe^{II}_aFe^{III}_bFe^{III}_c$. As a consequence of this large-amplitude motion the recoilless fraction of iron ions in the valence-detrapped Fe_3O complexes would be expected to be less than that for the Fe^{III} ions in the $Fe^{III}_2Co^{II}O$ complexes. This is the case even though both types of complexes are in the same lattice. The experimental ratio increases some from 0.930 at 200 K to 1.083 at 330 K probably because the whole crystalline lattice is becoming looser at the higher temperature.

It was reported[7d] previously that $[Fe_3O(O_2CCH_3)_6(py)_3](py)$ (**1**) shows a temperature-dependent Mössbauer spectrum. At temperatures below 112 K there are two doublets, a high-spin Fe^{II} doublet, and a high-spin Fe^{III} doublet in the area ratio of 1:2. A third quadrupole-split doublet appears suddenly at ~112 K as the sample temperature is increased. This third doublet corresponds to a valence-detrapped form of the Fe_3O complex. A valence-detrapped complex is one where the complex on the vibrational time scale (10^{-13} s) is trapped in one of its vibronic states but is rapidly interconvering (tunneling) between its three (or four) lowest energy vibronic states faster than the Mössbauer time scale (10^{-7}–10^{-8} s). The third doublet for complex **1** was found to correspond to 30–40% of the spectral area between 112 and 168 K. A further increase in temperature leads to additional changes in the spectrum for **1**, and by ~190 K there is only one doublet, the valence-detrapped doublet, present. These observations fit well with the heat capacity results[7h] for **1**, where there is a first-order phase transition seen at ~112 K, followed by a higher order phase transition that starts at ~113 K and culminates at ~190 K.

The temperature dependence of the Mössbauer spectrum of the solid solution **3** parallels that of Fe_3O complex **1**. There are only valence-trapped Fe_3O complexes in complex **3** at temperatures of 85 K or lower. These trapped complexes probably comprise a ferrodistortive phase I (vide infra) that is ordered. At 95 K we see the first appearance of the valence-detrapped third doublet. In analogy to complex **1**, at temperatures above 95 K complex **3** may be in the antiferrodistortive phase II, where there are two interpenetrating sublattices. Finally, at temperatures above ~200 K all Fe_3O complexes in complex **3** are valence detrapped. This could correspond to phase III, the paradistortive phase.

Solid-State ^{2}H NMR Spectroscopy. Solid-state ^{2}H NMR experiments were carried out on $[Fe_2CoO(O_2CCH_3)_6(C_5D_5N)_3](C_5D_5N)$ to investigate the nature of pyridine solvate motion. It was important to discover at what temperature(s) the solvate molecules experience a change in their level of dynamics and what types of motion they are undergoing. The deuterated pyridine form of complex **2** was studied in two different ways. In the first case the ^{2}H NMR sample was simply a polycrystalline sample. In the second case polycrystals were magnetically oriented in fluid eicosane by means of the 5.9-T magnet. After orientation, the hydrocarbon was cooled to room temperature to form a wax cube. In the case of an unoriented sample a powder spectrum is obtained where a distribution of resonance frequencies is seen reflecting the random distribution of orientations of molecules. If the quadrupolar interaction is axial in symmetry, then an axial powder pattern will be seen that has characteristic perpendicular and parallel "turning edges". When a molecule is oriented so that the external magnetic field is perpendicular to the C–D bond vector, resonance occurs at the "perpendicular edge". If the C–D vector is parallel to the external magnetic field, resonance occurs at the "parallel edge". For pyridine the separation in the perpendicular peaks is ~130 kHz, whereas the separation in the parallel peaks is ~260 kHz.[22] Obviously, the two perpendicular edge features

(22) (a) Rice, D. M.; Wittebort, R. J.; Griffin, R. G.; Meirovitch, E.; Stimson, E. R.; Meiwald, Y. C.; Freed, J. H.; Scheraga, H. A. *J. Am. Chem. Soc.* **1981**, *103*, 7707. (b) Meirovitch, E.; Belsky, I.; Vega, S. *J. Phys. Chem.* **1984**, *88*, 1522.

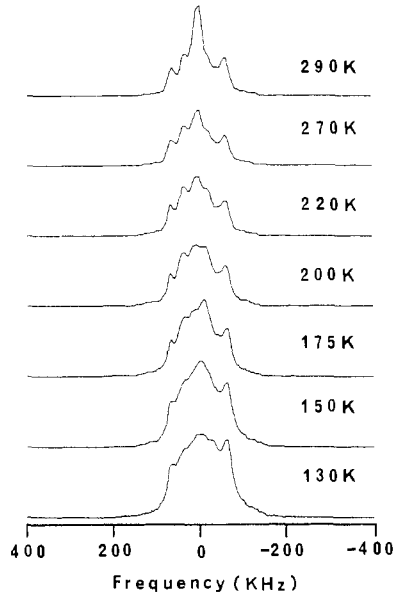

Figure 9. Temperature dependence of the solid-state ^2H NMR spectra for a polycrystalline (unoriented) powder sample of $[Fe_2CoO(O_2CCH_3)_6(C_5D_5N)_3](C_5D_5N)$.

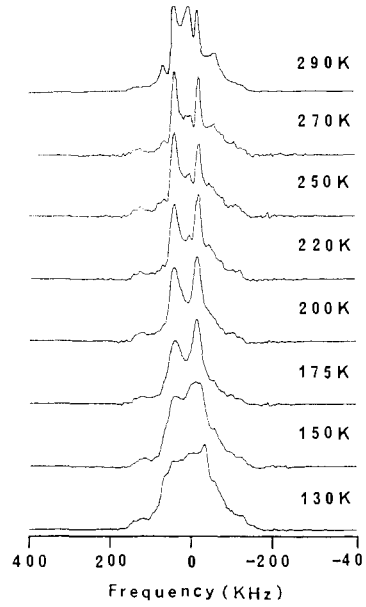

Figure 10. Temperature dependence of the solid-state ^2H NMR spectra of a magnetically oriented collection of ~20 microcrystals of $[Fe_2CoO(O_2CCH_3)_6(C_5D_5N)_3](C_5D_5N)$. The ~20 microcrystals were oriented in fluid eicosane with a 5.9-T field. After orientation the eicosane was cooled to form a wax cube where all microcrystals have their c axes aligned with the external magnetic field.

in a powder spectrum are much more intense than the two parallel edge features.

Temperature-dependent ^2H NMR spectra of **3** are shown in Figure 9 for an unoriented powder sample and in Figure 10 for a magnetically ordered sample. Our previous discussions[7a,c,d,e] of the characteristics of ^2H NMR spectroscopy of paramagnetic solids should be consulted. Such spectra show two effects, doublet quadrupolar splittings as well as paramagnetic shifts, arising from the dipolar coupling between the deuteron nuclear spin and magnetic moment due to the unpaired electrons of the paramagnetic metal complex. Due to the difficulty of refocusing simultaneously the quadrupolar and dipolar interactions in the solid echo pulse sequence, such spectra typically show intensity distortions. Our primary interest is to determine to what extent the solvate molecule is dynamically disordered from the quadrupolar splittings. Under the circumstances, this is readily estimated by the separation between fairly obvious spectral features such as the turning edges described above.

Examination of the spectra in Figure 9 clearly show the expected parallel (~260 kHz spitting) and perpendicular (~130 kHz splitting) edges for the static deuterons of the C_5D_5N ligands at all temperatures. The center of the powder spectra also shows an intense pattern with substantially reduced breadth and quadrupolar coupling. This pattern is assigned to the solvate deuterons, and the apparent maximum breadth, 60–70 kHz for $T > 175$ K, indicates a ~4-fold reduction of the quadrupolar splitting at high temperatures and thus a substantial degree of dynamic disorder.

Compared to our previous results with compound **1**,[7d] the spectra of Figure 10 show that compound **2** magnetically orients less well. Since this class of compounds orients with the crystallographic c axis (principal component of magnetic susceptibility tensor) parallel to the applied field, the ligand deuterons with their C–D bonds perpendicular to the c axis should appear as sharp lines with splittings near 140 kHz, as was observed for **1**.[7d] Since the maximum observed splittings approach the parallel edge frequencies, we conclude that the sample is only moderately oriented. Because a reduced quadrupolar coupling for the solvate molecule is seen, the lack of precise ordering is less troublesome. The solvate deteurons show for $T > 175$ K an intense and relatively sharp doublet with a splitting essentially equal to the maximum observed for the solvate in the powder spectra (Figure 9). This indicates that the solvate undergoes axially symmetric reorientation about the crystal c axis. Furthermore, the 4-fold reduction in the coupling indicated by the powder patterns (Figure 9) suggests the following model for the solvate dynamics in complex **2** in the high-temperature phase. First, in-plane ring rotation reduces the quadrupolar splitting to half the static value and also makes all five ring deteurons equivalent. Second, axial reorientation of the ring normal in a perpendicular fashion about the c axis gives an additional 2-fold reduction of the coupling and places the unique axis of the residual coupling tensor along the crystal c axis (stacking direction).

Reference to Figure 10 shows that as the deuterated sample of complex **2** is cooled, the solvate doublet remains well resolved down to ~175 K. Below this temperature the doublet broadens very substantially. Recall that the only phase transition in complex **2** occurs at ~148 K. It appears that it is at this temperature the axial reorientation of the C_5D_5N solvate molecules about the C_3 axis stops. However, even by 130 K it does *not* appear that the in-plane rotation of the solvate molecules about the pseudo-C_6 axis has completely stopped. Thus, the main conclusion of the ^2H NMR study of Fe_2CoO complex **2** is that the jumping of the pyridine solvate molecule about the C_3 axis cooperatively stops in the main ~148 K phase transition. However, there is a rotation of each pyridine solvate molecule about a local pseudo-C_6 axis that persists at temperatures below the ~148 K phase transition. This is in total agreement with the heat capacity results for Fe_2CoO complex **2**, which show a total entropy gain of ~R ln 3.

Effects of Quenched Disorder. There were two goals at the outset of this work. One was to see whether additional information on the nature of the phase transitions observed for $[Fe_3O(O_2CCH_3)_6(py)_3](py)$ could be obtained by cocrystallizing this complex with the permanently distorted Fe_2CoO complex. The second goal was aimed at discovering what type of impurity the Fe_2CoO complex is in the Fe_3O matrix. If the Fe_2CoO complex behaves as an inactive impurity (ie., a missing Fe_3O complex), then percolation theory gives a prediction as to the minimum amount of Fe_2CoO complexes needed to prevent the solid-solution matrix from becoming an ordered phase.

A brief review of the present theoretical modeling of the phase transitions in $[Fe_3O(O_2CCH_3)_6(py)_3](py)$ (**1**) is important. Stratt and Adachi[23] employed a spin Hamiltonian approach in a molecular field approximation of intermolecular interactions in **1**. The intermolecular pyridine–pyridine contacts in evidence in

(23) Stratt, R. M.; Adachi, S. H. *J. Chem. Phys.* **1987**, *86*, 7156.

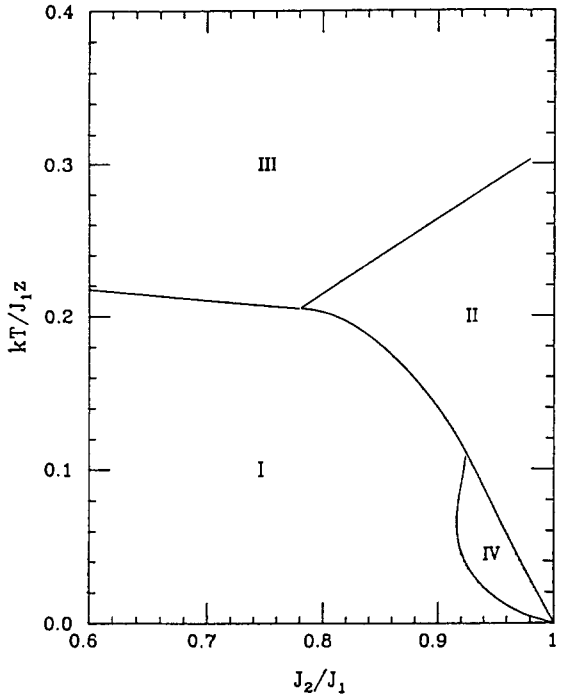

Figure 11. Phase diagram calculated by Stratt and Adachi,[24] employing a molecular field theory to account for the phase transitions in mixed-valence Fe_3O complexes that crystallize in the $R32$ space group. The vertical axis is temperature plotted in units of J_1z/k, where k is the Boltzmann constant, z is the number of Fe_3O complexes surrounding each Fe_3O complex, and J_1 is the interaction energy of two neighboring complexes, both of which are distorted parallel to each other. The horizontal axis is the ratio of the "antiferromagnetic" (J_2) to the "ferromagnetic" (J_1) coupling, where J_2 is the interaction energy for two neighboring complexes, one of which is distorted and the other is undistorted.

Figure 2 were parametrized with J_0 (taken as zero of energy), J_1, J_2, and J_3, which are respectively the energies of two neighboring Fe_3O complexes, both of which are undistorted, both of which are distorted parallel to each other, only one of which is distorted, and both of which are distorted but an an angle of $2\pi/3$ with respect to each other. The phase diagram pictured in Figure 11 resulted. Phases I–III are of the greatest interest. In phase I all Fe_3O complexes are valence trapped (distorted) and the sense of the distortion is aligned in domains. Phase I is the ferrodistortive phase. In analogy to magnetic systems, two interpenetrating sublattices develop in phase II. The A sublattice Fe_3O complexes are each surrounded by six B sublattice Fe_3O complexes and vice versa. There is an antiferrodistortive alignment of distorted Fe_3O complexes in sublattice A relative to those in the B sublattice. In phase III all complexes are rapidly interconverting between their three (our four) vibronic states. For a specific range of parameters where $J_1/J_2 = 0.8$–0.9, complex **1** is predicted upon heating from low temperature to undergo a first-order phase transition from phase I to II, followed by a higher order phase transition from phase II to III. These seem to occur at ~112 and ~190 K, respectively, for complex **1**. It must be cautioned that the influence of the pyridine solvate molecule was not factored into this theory.

Very recently Adachi et al.[14] developed new theoretical models in an effort to understand the effects of the quenched disorder in the solid solution $[Fe^{III}_2Fe^{II}_{1-x}Co^{II}_xO(O_2CCH_3)_6(py)_3](py)$. In general, randomly placed impurities interfere with the ability of a modulated phase to "lock in" on the regular structure of the underlying lattice.[24] It was anticipated that the Fe_2CoO complexes introduced into the Fe_3O lattice would have a stronger effect than mere vacancies. The Fe_2CoO complexes interact with their neighbors in a way that depends on the direction of distortion.

(24) *111-condensed Matter*; Balian, R., Maynard, R., Toulouse, G., Eds.; North-Holland: Amsterdam, 1979.

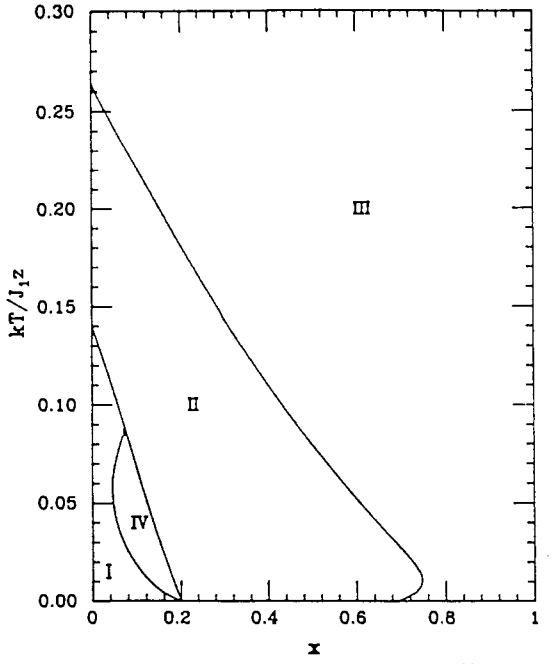

Figure 12. Phase diagram calculated by Adachi et al.,[14] employing a cluster mean-field theory to account for the phase transitions in the solid-solution $[Fe^{III}_2Fe^{II}_{1-x}Co^{II}_xO(O_2CCH_3)_6(py)_3](py)$. Reduced temperature is plotted versus the concentration x of Fe_2CoO complexes. The vertical axis is temperature plotted in units of J_1z/k, where k is the Boltzmann constant, z is the number of Fe_2MO (M = Fe, Co) complexes surrounding each Fe_2MO complex, and J_1 is the interaction energy of two neighboring complexes, both which are distorted parallel to each other. It was assumed that $J_2/J_1 = 0.90$ and $J_3/J_1 = 0.75$.

Ordering could be destroyed even before the percolation threshold is reached.

Adachi et al.[14] considered the substitution of Fe_2CoO complex for a Fe_3O complex as being equivalent to putting magnetic impurities into a spin model. They examined two models that highlighted the novel form of this quenched disorder. In model I an Ising antiferromagnet in which randomly chosen spins are quenched "up" was employed. Model II involved as Ising ferromagnet in which randomly chosen spins are quenched "up" or "down" with equal probability. Both models were studied with a cluster mean-field theory and via Monte Carlo simulation. In both cases anomalously long thermal relaxation times and a zero-temperature critical impurity concentration, which is *not* determined by percolation theory, were predicted. In Figure 12 is illustrated the mean-field virtual crystal phase diagram obtained by Adachi et al.[14] for the solid solution $[Fe^{III}_2Fe^{II}_{1-x}Co^{II}_xO(O_2CCH_3)_6(py)_3](py)$. In this diagram the reduced absolute temperature is plotted versus the concentration of Fe_2CoO complexes. Parameter ratios of $J_2/J_1 = 0.9$ and $J_3/J_1 = 0.75$ were assumed. From the diagram in Figure 12 it is clear that at zero temperature order is destroyed at a critical concentration of $x_c = 0.69$.

Some of the main predictions of the theoretical work of Adachi et al.[14] are (1) there is a critical concentration of Fe_2CoO complexes to destroy order in the solid-solution compound that is not predicted by purely percolative grounds and (2) a small concentration of Fe_2CoO complexes ought to be enough to decrease the rate of intramolecular electron transfer for the Fe_3O complexes in the lattice. These predictions and the phase diagram in Figure 12 can be compared to the experimental results presented in this paper, as well as the results of the previous DTA study.[7h]

Examination of the phase diagram in Figure 12 shows that for $[Fe^{III}_2Fe^{II}_{1-x}Co^{II}_xO(O_2CCH_3)_6(py)_3](py)$ with $x = 0.5$ there should be only a higher order phase transition from the antiferrodistortive phase II to the paradistortive phase III. However, in the plot of ΔC_P versus temperature (Figure 5) for the solid solution **3**, peaks indicating the existence of at least two phase transitions can be seen. Peaks are seen at 84.5, 148.0, and 168.8 K. Furthermore, there are clear indications in the Mössbauer spectra (Figure 8)

for complex **3** that it converts from totally valence trapped in phase I through a region where the third valence-detrapped doublet is present (phase II?) eventually to a region (phase III?) where all Fe_3O complexes are valence detrapped. These same types of changes in Mössbauer spectra were seen for the undoped Fe_3O complex **1**. Thus, in contrast to the predictions of Figure 12, it appears that the $x = 0.5$ complex does access the ferrodistortive phase I. A larger concentration of cocrystallized Fe_2CoO complexes is needed in order to avoid the apparently ferrodistortively ordered phase I. It will take considerable additional experiments before the critical concentration x_c can be evaluated. DTA results[7h] indicated that the lowest temperature thermal effect (84.5 K for $x = 0.50$) could not be seen for a solid with $x = 0.60$. However, as can be seen in Figure 5, the various thermal effects become quite broad and difficult to detect as x increases. Perhaps Mössbauer data will be more useful in determining x_c.

There is one other aspect of the experimental data that should be noted. There is a phase transition at 148.5 K in the undoped Fe_2CoO complex **2**. From the heat capacity and solid-state ^2H NMR data this phase transition primarily involves the onset of motion of the pyridine solvate molecules. There is enough communication between a given solvate molecule in one lattice site with its neighboring solvate molecules that there is a somewhat cooperative onset of each solvate molecule reorienting about the C_3 axis even though there is no direct contact between pairs of pyridine solvate molecules. Solvate–solvate intermolecular interactions must be propagated via py···Fe_2CoO···py pathways. Thus, the interaction between a given Fe_2CoO complex and the two nearby solvate molecules must be appreciable. The influence of solvate molecules on the phase transitions in these complexes needs to be included in a theory developed for the phase transitions in these complexes. In this sense it is important to remember that $[Fe_3O(O_2CCH_3)_6(py)_3]$, a complex without solvate molecules, has been reported[7f] to remain completely valence trapped up to the highest temperature (315 K) at which it has been examined.

Acknowledgment. We are grateful for support from National Institutes of Health Grant HL13652 (D.N.H.) and National Science Foundation Grants DMB-8606358 (R.J.W.).

Supplementary Material Available: Tables 11, 21, 31, 41, 51, 12, 22, 32, 42, 52, and 72, listing atom coordinates, bond distances, bond angles, anisotropic thermal parameters, hydrogen atom coordinates, and complete crystallographic data for $[Fe_3O(O_2CCH_3)_6(py)_3](py)$ (**1**) and for $[Fe_2CoO(O_2CCH_3)_6(py)_3](py)$ (**2**) (6 pages); Table 61 and 62, listing structure factors for complexes **1** and **2** (15 pages). Ordering information is given on any current masthead page.

Contribution from the Department of Chemistry, Memorial University of Newfoundland, St. John's, Newfoundland, Canada A1B 3X7, and National Research Council, Ottawa, Ontario, Canada K1A OR6

Binuclear Metallacyclic Copper(II) Complexes with a Large Unoccupied Cavity Derived from a Tetradentate, Nonmacrocyclic Polyhydroimidazole Ligand†

Sanat K. Mandal,[1a] Laurence K. Thompson,*[1a] Michael J. Newlands,[1a] Eric J. Gabe,[1b] and Florence L. Lee[1b]

Received September 20, 1989

The potentially tetradentate ligand 1,2,4,5-tetrakis(4,5-dihydroimidazol-2-yl)benzene (BTIM) forms bischelating binuclear square-pyramidal copper(II) complexes in which two ligands and two metals form a metallacyclic structure with a very large, unoccupied cavity. The cavity is defined by a large copper–copper separation (Cu–Cu = 7.610 Å in $[Cu_2(BTIM)_2Cl_2]Cl_2·7H_2O$ (I); Cu–Cu = 7.30 and 7.42 Å in $[Cu_2(BTIM)_2(N_3)_2](N_3)_2·5H_2O$ (II)) and a large separation between the two parallel, eclipsed benzene rings (3.93 Å (I), 4.4 and 4.3 Å (II)). Variable-temperature magnetism and ESR spectra support the presence of very weak antiferromagnetic exchange between the copper (II) centers in I and II. The crystal and molecular structure of the complex $[Cu(LP)_2](ClO_4)_2$ (IV) (LP = 1,2-bis(4,5-dihydroimidazol-2-yl)benzene) is also reported. LP represents half of the ligand BTIM. IV crystallized in the monoclinic system, space group $P2_1/n$, with $a = 10.4569$ (5) Å, $b = 11.1376$ (8) Å, $c = 12.6854$ (7) Å, $\beta = 98.500$ (10)°, and two formula units per unit cell. Refinement by full-matrix least squares gave final residuals of $R = 0.060$ and $R_w = 0.067$. The mononuclear copper center in IV is square planar, involving two bidentate ligands.

Introduction

Polyfunctional ligands involving benzimidazole, benzothiazole, and hydroimidazole functional groups (and derivatives thereof) can be synthesized simply by condensation of appropriate nitriles with *o*-phenylenediamine, (*o*-aminobenzene)thiol, and ethylenediamine, respectively (or derivatives thereof). Examples of such bidentate ligands and their cobalt(II), nickel(II), copper(II), and zinc(II) complexes have already been reported.[2-5] These ligands were derived from phthalonitrile, and the complexes were found to be mostly mononuclear. Our interest in polynuclear complexes led us to investigate similar derivatives obtained from the tetranitrile 1,2,4,5-tetracyanobenzene, and in the present study copper(II) complexes of the ligand 1,2,4,5-tetrakis(4,5-dihydroimidazol-2-yl)benzene (BTIM) (Figure 1) are reported. The juxtaposition of the hydroimidazole rings would suggest a preference for the formation of binuclear derivatives, and this has been demonstrated for the complexes $[Cu_2(BTIM)_2X_2]X_2·yH_2O$ (X = Cl, $y = 7$ (I); X = N_3, $y = 5$ (II)). However, contrary to what was expected, the structures involve two essentially parallel ligands bridging the two copper centers, which create a large, empty cavity with a large copper–copper separation (>7.3 Å). Binuclear coordination complexes involving cavity structures, with essentially isolated metal centers separated by large distances (>5 Å), usually involve large, macromonocyclic and -polycyclic ligands, which essentially encapsulate the two metals.[6,7] Macropolycyclic cryptand ligands involving nitrogen and sulfur donors generate binuclear copper(II) derivatives of this sort, in which the copper centers display reversible monoelectronic, simultaneous reduction at identical, positive potentials. The ligand 1,7,13,19-tetraaza-4,16-dioxa-10,22,27,32-tetrathiatricyclo[17.5.5.5^{7,13}]tetratriacontane forms a binuclear copper(II) complex that exhibits a single reduction wave at $E_{1/2} = 0.200$ (5) V vs SCE[8-11] and involves

* To whom correspondence should be addressed.
† This paper assigned NRCC Contribution No. 31247.

(1) (a) Memorial University. (b) National Research Council.
(2) Lever, A. B. P.; Ramaswamy, B. S.; Simonsen, S. H.; Thompson, L. K. *Can. J. Chem.* **1970**, *48*, 3076.
(3) Rendell, J. C. T.; Thompson, L. K. *Can. J. Chem.* **1979**, *57*, 1.
(4) Thompson, L. K.; Rendell, J. C. T.; Wellon, G. C. *Can. J. Chem.* **1982**, *60*, 514.
(5) Wellon, G. C.; Bautista, D. V.; Thompson, L. K.; Hartstock, F. W. *Inorg. Chim. Acta* **1983**, *75*, 271.
(6) Fenton, D. E. *Adv. Inorg. Bioinorg. Mech.* **1983**, *2*, 187.
(7) Lehn, J.-M. *Pure Appl. Chem.* **1980**, *52*, 2441.

0020-1669/90/1329-3556$02.50/0